Polarization-induced interference within electromagnetically induced transparency for atoms of double-V linkage

Yuan Sun,[1,*] Chang Liu,[2] Ping-Xing Chen,[1] and Liang Liu[3,†]

[1]*Interdisciplinary Center for Quantum Information, National University of Defense Technology, Changsha 410073, People's Republic of China*

[2]*Institute for Quantum Computing and Department of Physics & Astronomy, University of Waterloo, Waterloo, Ontario, Canada N2L 3G1*

[3]*Key Laboratory of Quantum Optics and Center of Cold Atom Physics, Shanghai Institute of Optics and Fine Mechanics, Chinese Academy of Sciences, Shanghai 201800, People's Republic of China*

(Received 6 September 2017; published 12 February 2018)

People have been paying attention to the role of atoms' complex internal level structures in the research of electromagnetically induced transparency (EIT) for a long time, where the various degenerate Zeeman levels usually generate complex linkage patterns for the atomic transitions. It turns out, with special choices of the atomic states and the atomic transitions' linkage structure, clear signatures of quantum interference induced by the probe and coupling light's polarizations can emerge from a typical EIT phenomena. We propose to study a four-state system with double-V linkage pattern for the transitions and analyze the polarization-induced interference under the EIT condition. We show that such interference arises naturally under mild conditions on the optical field and atom manipulation techniques. Moreover, we construct a variation form of double-M linkage pattern where the polarization-induced interference enables polarization-dependent cross modulation between incident weak lights that can be effective even at the few-photon level. The theme is to gain more insight into the essential question: how can we build a nontrivial optical medium where incident lights experience polarization-dependent nonlinear optical interactions, valid for a wide range of incidence intensities down to the few-photon level?

DOI: 10.1103/PhysRevA.97.023815

I. INTRODUCTION

Ever since the early days of investigating EIT and four-wave mixing (FWM) in atomic mediums, it has been noticed that the effects of the multiple Zeeman sublevels cannot be overlooked [1–6]. Under special scenarios such a multistate system with complicated linkage structure can be transformed back into a simple three-level EIT system [7–9], while typically it leads to complexities in the EIT or FWM processes which usually exhibit strong correlations with the polarizations of the incident light [4,5,10–13]. Investigations into these effects have already led to a few interesting findings, such as the controlled rotation of the polarization of an incident optical pulse [10], manipulation of the transparency window [5,12,14], vector magnetometry from EIT in linearly polarized light [15], and controlling enhancement or suppression of FWM by polarized light [4]. Of particular importance is the construction of quantum memory for photon polarization states via utilizing those Zeeman sublevels [16,17]. Those previous investigations have paved the way for studying the quantum interference induced by the polarizations of the driving lasers with special linkage geometry of atomic states in optically thick medium formed by cold alkali-metal atoms.

Meanwhile, generating and manipulating nonlinear interactions between optical fields of low intensities at the few-photon level is of essential importance in the research frontier of quantum optics [18]. According to early predictions of Harris and Hau, large cross-phase shifts through enhancing the weak Kerr effect by EIT at very low light intensities down to the single-photon level are hardly attainable [19]. In particular, a lot of effort has been devoted to enhancement of the nonlinear interaction between single photon pulses via high-finesse cavity [20–22] or Rydberg blockade [23–25]. Moreover, people are trying to seek novel schemes based upon EIT and FWM for cross modulation at the single-photon level without invoking the experimental complexities of high-Q cavities or Rydberg atoms. Much exciting progress has been achieved along this direction, including the double slow light method in a multilevel system [26,27], stationary light method [28], and especially the recent developments of cross-phase modulation (XPM) via FWM of double-Λ configuration in a three-level system [29] or four-level system [30]. Although the photonic polarization degree of freedom has not been explicitly brought into these XPM schemes so far, they have naturally triggered the motivation of introducing polarization-dependent nonlinear interactions between optical fields of low intensities down to the few-photon level via EIT and FWM methods.

In this article, we discuss the polarization-induced quantum interference under the general EIT condition in a special double-V linkage structure of atomic internal electronic states, which can be realized in ^{87}Rb atoms. We demonstrate in theory that this interference is inherently associated with the polarization degree of freedom, has clear physical signature, and can be observed with moderate experimental conditions. Then we extend this concept to a multistate system with double-M linkage structure, where we construct a mechanism of polarization-dependent cross modulation between two weak incident optical fields. The proposed mechanism is in principle

*sunyuan17@nudt.edu.cn
†liang.liu@siom.ac.cn

applicable to very low incident intensities such as a weak coherent light pulse containing energy equivalent to only a few photons. Throughout this article, the atom-light interaction is treated with the one-dimensional approximation [31,32], where effectively only one transverse spatial mode of the optical fields is taken into consideration. In the Appendixes, we include details of derivations and more examples from numerical simulations omitted in the main text. First we offer a discussion of the relatively simple case of polarization-induced quantum interference in a four-state system of double-V linkage structure without spontaneous emission in Appendix A. Then we provide more analysis and more examples for EIT with the double-V linkage structure under the presence of decoherences in Appendix B. Finally, we present more details about the atom-light interaction with the double-M linkage structure, focusing on the polarization-dependent dynamics between two weak copropagating optical fields in Appendix C.

II. DOUBLE-V LINKAGE STRUCTURE

To begin with, consider an EIT process where the polarizations of the probe and coupling lights are resolved such as Figs. 1(a) and 1(b), where an optical pumping process

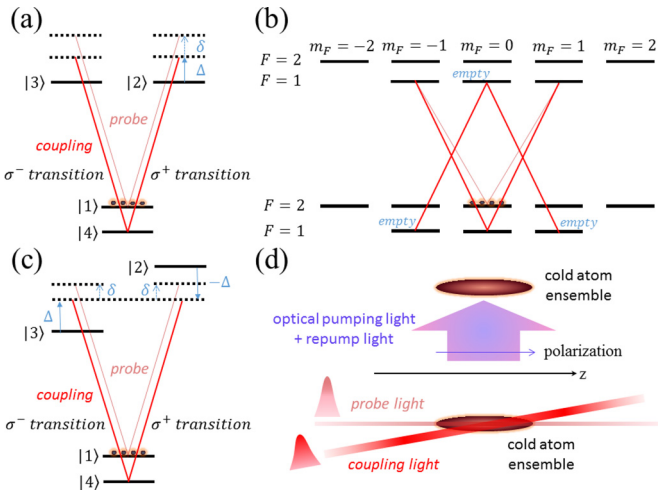

FIG. 1. Polarization-resolved configuration of EIT in atoms with double-V linkage pattern. (a) Schematic of the double-V linkage structure of a simplified four-state system where the two excited states are degenerate in energy. The k vectors of incident coupling and probe lights are along the z direction such that they couple to the σ^+ transitions and σ^- transitions, respectively. The probe beam is assumed to have relatively low intensity; hence it does not disturb the population of state $|1\rangle$. (b) Implementation of the abstracted double-V linkage structure in ^{87}Rb $D1$ or $D2$ transitions, where $|1\rangle$ and $|4\rangle$ are realized by the two magnetic insensitive clock states while $|2\rangle$ and $|3\rangle$ are realized in the manifold of the $5P$ level. It can also be implemented in the Rydberg EIT system [6]; see Appendix B. (c) A double-V linkage structure where $|2\rangle$ and $|3\rangle$ are not degenerate in energy. (d) Simplified proposal for experimental implementation. The cold atom ensemble goes through an optical pumping process at the beginning, which prepares the initial state as $|F = 2, m_F = 0\rangle$ of the ground level. Typically, the coupling laser is cw and the incident probe light takes the form of an optical pulse. Probe beam and coupling beam are assumed to be parallel and overlapping, or with a tiny angle for the purpose of phase matching in the medium if desired.

concentrates the initial population into state $|1\rangle$. The state initialization is necessary to remove the requirement of $J = 0$ of Ref. [5] which severely limits the choice of atoms to special ones like thallium. When the probe light intensity is weak, its equation of motion (EOM) up to the first order can be derived from the Maxwell-Bloch equations in the rotating wave frame as the following:

$$\frac{\partial}{\partial z}\Omega_{p+} + \frac{1}{c}\frac{\partial}{\partial t}\Omega_{p+} = i\frac{n\sigma\Gamma}{2}\rho_{21}, \tag{1a}$$

$$\frac{\partial}{\partial z}\Omega_{p-} + \frac{1}{c}\frac{\partial}{\partial t}\Omega_{p-} = i\frac{n\sigma\Gamma}{2}\rho_{31}, \tag{1b}$$

$$\frac{d}{dt}\rho_{21} = \frac{i}{2}\Omega_{p+} - \frac{i}{2}\frac{\Omega_c}{\sqrt{2}}\rho_{41} + \left(i(\Delta+\delta) - \frac{\Gamma}{2}\right)\rho_{21}, \tag{1c}$$

$$\frac{d}{dt}\rho_{31} = \frac{i}{2}\Omega_{p-} + \frac{i}{2}\frac{\beta_c\Omega_c}{\sqrt{2}}\rho_{41} + \left(i(\Delta+\delta) - \frac{\Gamma}{2}\right)\rho_{31}, \tag{1d}$$

$$\frac{d}{dt}\rho_{41} = -\frac{i}{2}\frac{\Omega_c^*}{\sqrt{2}}\rho_{21} + \frac{i}{2}\frac{\beta_c^*\Omega_c^*}{\sqrt{2}}\rho_{31} + \left(i\delta - \frac{\gamma}{2}\right)\rho_{41}, \tag{1e}$$

where subscripts p and c stand for probe and coupling lights, respectively, Δ is the one-photon detuning, δ is the two-photon detuning, Γ is the decay rate of $|2\rangle$ and $|3\rangle$ where the dominant decay channel is regarded as the spontaneous decay to the ground levels, γ is the decoherence rate between $|1\rangle$ and $|4\rangle$, n is the atom density, and σ is the atom-light cross section for the probe light. $\Omega_{p+}, \frac{\Omega_c}{\sqrt{2}}$ are the Rabi frequencies for the σ^+ transitions, while $\Omega_{p-}, \frac{\beta_c\Omega_c}{\sqrt{2}}$ are the Rabi frequencies for the σ^- transitions, with $|\beta_c| = 1$. Namely, the coupling light is assumed to be linearly polarized with decomposition via the circular polarization basis: $P_c = \frac{1}{\sqrt{2}}(P_+ + \beta_c P_-)$. This assumption of linear polarization is not necessary and the analysis below can be easily extended to any polarization state of the coupling light; see Appendix B for further details.

We examine the propagation of the probe beam through the cold atom medium of finite optical depth (OD) along the z direction, by solving for the steady-state solution of Eq. (1) [33], where we eliminate the terms of time derivatives; then the equation governing the dynamics of the probe light's two polarization components is obtained as the following:

$$\frac{d}{dz}\begin{bmatrix}\Omega_{p+}\\ \Omega_{p-}\end{bmatrix} = \frac{i}{2}n\sigma\Gamma A^{-1}\begin{bmatrix}\Omega_{p+}\\ \Omega_{p-}\end{bmatrix}, \tag{2}$$

where A is a 2×2 matrix independent of z, with $A_{11} = A_{22} = \frac{\Omega_c^2}{2(2\delta+i\gamma)} - 2\Delta - 2\delta - i\Gamma$, $A_{12} = -\beta_c^*\frac{\Omega_c^2}{2(2\delta+i\gamma)}$, and $A_{21} = -\beta_c\frac{\Omega_c^2}{2(2\delta+i\gamma)}$.

The matrix A has eigenvalues λ_1, λ_2 as in the following equation; therefore, Eq. (2) can be decoupled into two independent branches which correspond to two types of different propagation dynamics of the probe light:

$$\lambda_1 = -2\Delta - 2\delta - i\Gamma, \tag{3a}$$

$$\lambda_2 = \frac{\Omega_c^2}{2(2\delta + i\gamma)} - 2\Delta - 2\delta - i\Gamma. \tag{3b}$$

From Eq. (3), an observation can be made that λ_1 is tied to dynamics similar to a two-level atom (TLA), while λ_2 is tied to dynamics similar to typical EIT. Upon incidence, the

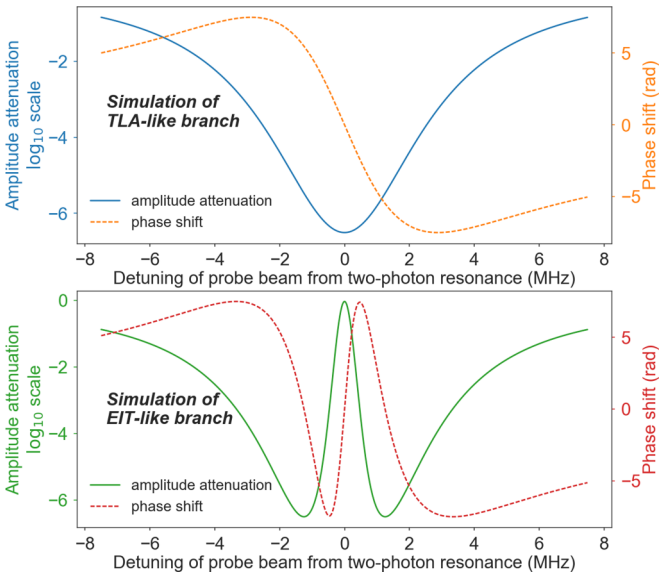

FIG. 2. Numerical simulation for the dispersion of the probe beam after propagation in the optically dense cold atom ensemble (OD = 30), where the atomic structure and coupling laser linkage pattern are according to Fig. 1(a). The upper graph is for the TLA-like branch, and the lower graph is for the EIT-like branch. The solid lines are for absorption while the dashed lines are for phase shift. The atomic parameters are $\Gamma = 2\pi \times 5.75$ MHz, which is from ^{87}Rb $D1$ transition, $\gamma = 0.001 \times \Gamma$, and the optical parameters are $\Omega_c = 2\pi \times 2.5$ MHz, $\Delta = 0$.

probe light decomposes into two components with opposite polarizations: $\frac{1}{\sqrt{2}}(\Omega_{p+} + \beta_c^* \Omega_{p-})$ is the projection onto the TLA branch and $\frac{1}{\sqrt{2}}(-\Omega_{p+} + \beta_c^* \Omega_{p-})$ is the projection onto the EIT branch. In general, the polarization ingredients for probe light of the two branches are solely determined by the coupling light's polarization. Loosely speaking, the coupling light induces birefringence in the medium such that for the probe laser, the medium is transparent to one polarization component but opaque to the other. This process can also be equivalently interpreted from the FWM viewpoint. An example of numerical simulation is shown in Fig. 2. We note that the assumption of weak probe light pulse intensity is important in the above derivations for the following reason. During the interaction, when the dissipation of the probe light takes place, some population will be possibly pumped into some magnetic sublevels other than $|F = 2, m_F = 0\rangle$ by spontaneous emission. Under the weak probe light assumption, this population displacement is tiny and its effect of backaction onto the probe light can be safely neglected.

Due to the energy degeneracy of the states $|2\rangle, |3\rangle$, the level structure of Fig. 1(a) possesses a special symmetry from the viewpoint of the Morris-Shore transform [7,8]. Therefore, it is necessary to examine the case where this symmetry is broken, namely with the energy degeneracy lifted. This triggers the study of a linkage structure shown in Fig. 1(c), where the energies of $|2\rangle$ and $|3\rangle$ differ by $2\hbar\Delta$ and the frequency of the coupling light is naturally chosen to correspond to the energy difference from $|4\rangle$ to the middle of $|2\rangle$ and $|3\rangle$. This special linkage structure can also be implemented according to Fig. 1(b) within ^{87}Rb $D1$ or $D2$ transitions, where an extra magnetic field along the z direction can be applied to lift the energy degeneracy of $|2\rangle$ and $|3\rangle$. When the applied magnetic field is of reasonably moderate strength, only the first-order Zeeman shift needs to be considered and the energy shift of relevant states with $m_F = 0$ can be effectively treated as zero.

Formally, assuming that the probe pulse duration τ is long enough such that $|\tau \cdot \Delta| \gg 1, |\tau \cdot \Omega_c| \gg 1$; then the EOM for the system is given by the Maxwell-Bloch equations almost identical to Eq. (1), with an essential difference of $\Delta \to -\Delta$ in Eq. (1c). After applying the steady-state condition, the equation governing the dynamics of the probe light's propagation through the medium is

$$\frac{d}{dz}\begin{bmatrix}\Omega_{p+}\\ \Omega_{p-}\end{bmatrix} = \frac{i}{2} n\sigma\Gamma B^{-1}\begin{bmatrix}\Omega_{p+}\\ \Omega_{p-}\end{bmatrix}, \tag{4}$$

where B is a 2×2 matrix independent of z, with $B_{11} = \frac{\Omega_c^2}{2(2\delta + i\gamma)} + 2\Delta - 2\delta - i\Gamma$, $B_{12} = -\beta_c^* \frac{\Omega_c^2}{2(2\delta+i\gamma)}$, $B_{21} = -\beta_c \frac{\Omega_c^2}{2(2\delta+i\gamma)}$, and $B_{22} = \frac{\Omega_c^2}{2(2\delta+i\gamma)} - 2\Delta - 2\delta - i\Gamma$.

Eventually the characteristics of Eq. (4) can be studied via analyzing B, whose eigenvalues are the following:

$$\lambda_\pm = \frac{|\Omega_c|^2}{2(2\delta + i\gamma)} - 2\delta - i\Gamma \pm \sqrt{4\Delta^2 + \left(\frac{|\Omega_c|^2}{2(2\delta + i\gamma)}\right)^2}. \tag{5}$$

Analogously, Eq. (4) can be decoupled into two independent branches with different dispersion relations for the incident probe light. Although $\lambda_\pm$ are of quite different appearances compared with Eq. (3), we can still identify that one is associated with a TLA scattering behavior branch while the other one is associated with an EIT scattering behavior branch. To explain this classification, we first examine the situation with $\delta = 0$, where Eq. (4) is reduced to

$$\frac{d}{dz}(-\beta_c \Omega_{p+} + \Omega_{p-}) = 0, \tag{6a}$$

$$\frac{d}{dz}(\beta_c \Omega_{p+} + \Omega_{p-}) = -\frac{n\sigma}{2}(\beta_c \Omega_{p+} + \Omega_{p-}). \tag{6b}$$

For $\delta \neq 0$, we invoke the approximation that $|\delta|$ is small such that $|\Omega_c|^2 \gg |2\Delta \cdot 4\delta|$ and $\gamma = 0$, which leads to $\sqrt{4\Delta^2 + (\frac{|\Omega_c|^2}{4\delta})^2} \approx \frac{|\Omega_c|^2}{4\delta} + \frac{8\delta\Delta^2}{|\Omega_c|^2}$. Then to the lowest order, $\lambda_+ \approx \frac{|\Omega_c|^2}{2\delta} - 2\delta - i\Gamma$, while $\lambda_- \approx -2\delta - i\Gamma$. The two branches' behaviors are EIT-like and TLA-like, respectively, and henceforth the previous observation is justified. A numerical simulation is presented in Fig. 3. In general, if the energy degeneracy of two excited states with different angular momentum is lifted, the polarization decomposition into the two branches of the incident probe beam is subject to not only the polarization of the coupling light but also its detuning, although the signature of polarization-induced interference persists. One possible application of an experimental realization of Fig. 1(c) is the precision measurement of the relative Zeeman shifts experienced by the excited states $|2\rangle, |3\rangle$.

III. DOUBLE-M LINKAGE STRUCTURE

Ideally, all-optical control and switching in the polarization degree of freedom and polarization filtering can be implemented by utilizing the double-V linkage structure of Fig. 1.

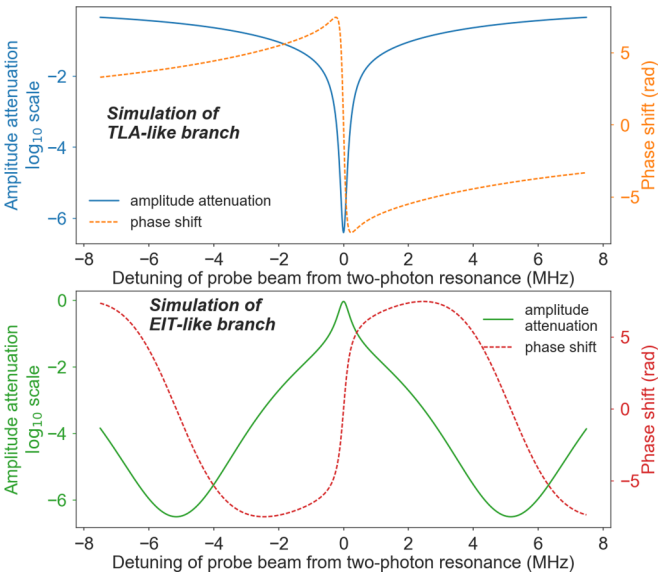

FIG. 3. Numerical simulation for the dispersion of the probe beam after propagation in the optically dense cold atom ensemble (OD = 30), where the atomic structure and coupling laser linkage pattern are according to Fig. 1(c). The upper graph is for the TLA-like branch and the lower graph is for the EIT-like branch. The solid lines are for absorption while the dashed lines are for phase shift. The atomic parameters are $\Gamma = 2\pi \times 5.75$ MHz, which is from ^{87}Rb $D1$ transition, $\gamma = 0.001 \times \Gamma$, $\Delta = 2\pi \times 5$ MHz, and the optical parameters are $\Omega_c = 2\pi \times 2.5$ MHz. Note that in the neighborhood of $\delta = 0$ the behavior is similar to that of Fig. 2.

Nevertheless, it requires the coupling light intensity to be much higher above the single-photon level. If one insists on coupling light of low intensity, then some form of enhancement such as a high finesse optical cavity has to be employed. Otherwise, modifications to the double-V linkage are in need to pursue polarization-induced interference within EIT and FWM processes between two weak optical fields.

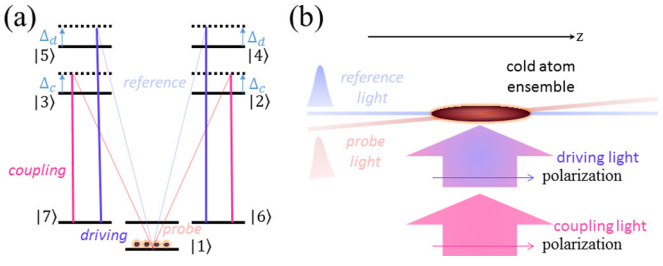

FIG. 4. (a) Schematic of the double-M linkage structure of a four-level seven-state system. It can be realized in the ^{87}Rb $D1$ or $D2$ transitions; see also Appendix C. (b) Simplified proposal for experimental implementation of the optical configuration. The reference and probe lights are almost parallel with a possible tiny cross angle for the purpose of phase matching. The coupling and driving lasers are assumed to be cw, of the same spatial mode, uniform in intensity across the cold atom ensemble and cross the probe and reference optical axis at right angle. The atoms are assumed to be cold enough such that the inhomogeneous broadening caused by atomic motion can be neglected.

In particular, consider the polarization-discriminating cross-modulation process according to configurations shown in Fig. 4, where the linkage structure enables double EIT for both the σ^+,σ^- transitions. The coupling and driving lasers are of moderate Rabi frequencies comparable to the linewidth of the transitions, while the incident probe and reference light pulses are of very low optical intensities. The driving and coupling lasers are essentially of the same physical nature even though they are different in frequencies. Both of them are narrow linewidth cw lasers shining onto the cold atom ensemble with a well-defined linear polarization.

Then, up to a global phase, the dynamics up to the lowest order can be derived from the Maxwell-Bloch equations [29,30,34] in the rotating wave frame, where the polarization is resolved with respect to the quantization axis choice as the z direction:

$$\frac{\partial}{\partial z}\Omega_{p+} + \frac{1}{c}\frac{\partial}{\partial t}\Omega_{p+} = i\frac{n\sigma_p\Gamma_c}{2}\rho_{21}, \tag{7a}$$

$$\frac{\partial}{\partial z}\Omega_{r+} + \frac{1}{c}\frac{\partial}{\partial t}\Omega_{r+} = i\frac{n\sigma_r\Gamma_d}{2}\rho_{41}, \tag{7b}$$

$$\frac{d}{dt}\rho_{21} = \frac{i}{2}\Omega_{p+} + \frac{i}{2}\Omega_c\rho_{61} + \left(i\Delta_c - \frac{\Gamma_c}{2}\right)\rho_{21}, \tag{7c}$$

$$\frac{d}{dt}\rho_{41} = \frac{i}{2}\Omega_{r+} + \frac{i}{2}\Omega_d\rho_{61} + \left(i\Delta_d - \frac{\Gamma_d}{2}\right)\rho_{41}, \tag{7d}$$

$$\frac{d}{dt}\rho_{61} = \frac{i}{2}\Omega_c^*\rho_{21} + \frac{i}{2}\Omega_d^*\rho_{41} - \frac{\gamma}{2}\rho_{61}, \tag{7e}$$

where Γ_c is the decay rate of states $|2\rangle$,$|3\rangle$, Γ_d is the decay rate of states $|4\rangle$,$|5\rangle$, γ is the decoherence rate of states $|6\rangle$,$|7\rangle$, which is typically tiny, and $\sigma_{p,r}$ are the atom-light cross sections for the probe and reference lights. The EOMs for Ω_{p-} and Ω_{r-} are of the same form with the following replacements: $\rho_{21} \to \rho_{31}$, $\rho_{41} \to \rho_{51}$, $\rho_{61} \to \rho_{71}$.

An inherent symmetry about polarization can be observed in the atom-light interaction with this atomic linkage structure. Equation (7) is now written with the circular polarization basis; nevertheless its form is invariant under the Morris-Shore transform to any orthonormal polarization basis; see also Appendix C. This symmetry is closely tied to the observation that the polarization-induced interference considered here is only up to the relative polarization difference of the probe and reference while no special polarization orientation preexists in the system.

We analyze the dynamics via the steady-state solution of Eq. (7) under the assumption of perfect ground-level coherence $\gamma = 0$ and equivalent detunings $\Delta_c = \Delta_d = \Delta$. The steady-state solution is useful when the incident pulse duration is very long such that an effective single frequency description is adequate. Then the dynamics of the probe and reference lights is specified by the following equation:

$$\frac{d}{dz}\begin{bmatrix}\Omega_{p\pm}\\ \Omega_{r\pm}\end{bmatrix} = \xi \underbrace{\begin{bmatrix} -\frac{\Omega_d}{\Omega_c}\Gamma_c & \Gamma_c \\ \frac{\Omega_d\Omega_c^*}{\Omega_d^*\Omega_c}\Gamma_d a_r & -\frac{\Omega_c^*}{\Omega_d^*}\Gamma_d a_r \end{bmatrix}}_{M_0} \begin{bmatrix}\Omega_{p\pm}\\ \Omega_{r\pm}\end{bmatrix}, \tag{8}$$

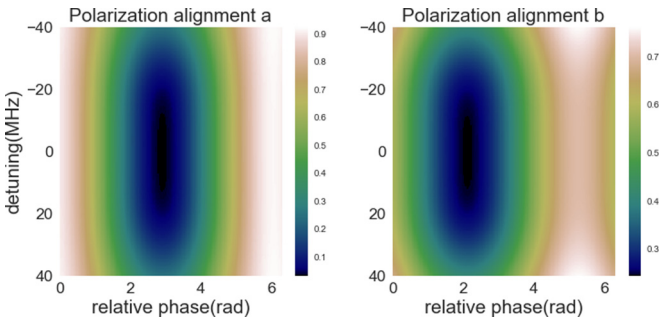

FIG. 5. Numerical simulation for the cross modulation between probe and reference incidences after propagation in an optically dense cold atom ensemble (OD = 10), where the atomic structure and controlling lasers are set according to Fig. 4. The total emergent intensity is plotted with normalization to the total incident intensity, where the incident probe and reference beams are assumed to be linearly polarized and at the same intensity. At alignment a, the angle between two linear polarizations is $\frac{\pi}{6}$, while at alignment b the angle is $\frac{2\pi}{3}$. The relative phase between the two lights is scanned, which is defined with respect to their left circular polarization component. The atomic parameters are $\Gamma_c = \Gamma_d = \Gamma = 2\pi \times 6.07$ MHz, which is from ^{87}Rb $D2$ transition, $\gamma = 0.01 \times \Gamma$, and the optical parameters are $\Omega_c = \Omega_d = 2\pi \times 5$ MHz, where the detuning Δ is scanned.

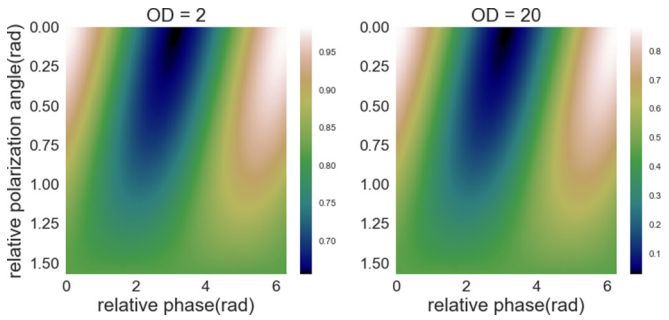

FIG. 6. Numerical simulation for the cross modulation between probe and reference incidences after propagation in an optically dense cold atom ensemble with OD = 2 and 20, with the same atomic parameters and coupling and driving Rabi frequencies as Fig. 5. The difference is that the detunings are fixed here: $\Delta = 5$ MHz, while the relative phase and relative polarization angle is scanned. Note that when the polarizations of the probe and reference lights are orthogonal, the scanning of the relative phase does not cause any change in the total emergent intensity.

with the constants ξ and a_r defined as

$$\xi = -\frac{n\sigma_p}{4}\frac{1}{\frac{\Omega_d}{\Omega_c}\left(i\Delta - \frac{\Gamma_c}{2}\right) + \frac{\Omega_c^*}{\Omega_d^*}\left(i\Delta - \frac{\Gamma_d}{2}\right)}, \quad a_r = \frac{\sigma_r}{\sigma_p}, \tag{9}$$

where we can further assume that $\Gamma_c = \Gamma_d = \Gamma$ typically.

For appropriate settings of control parameters, this system can demonstrate cross-modulation capabilities for the probe and reference lights involving the polarization degree of freedoms, provided the optical depth along the propagation axis is adequate.

In particular, we first analyze the two extreme cases where the polarization states of the probe and reference beams are identical or orthogonal. If their polarization states are identical, the situation reduces to that of a typical FWM, where the cross modulation is subject to their initial relative phase difference, just as Refs. [29,30]. If the polarizations of the incident probe and reference lights are orthogonal $\Omega_{r+}(0)\Omega_{p+}^*(0) + \Omega_{r-}(0)\Omega_{p-}^*(0) = 0$, then their initial phase difference does not contribute to their total transmitted power. To observe this, we can simply take a Morris-Shore transform such as that in the transformed new polarization basis $\Omega'_{p-}(0) = \Omega'_{r+}(0) = 0$, where $'$ denotes quantities expressed in the new basis.

More specifically, we discuss the cross modulation of amplitude, and the results of numerical simulations are presented in Figs. 5 and 6. These numerical simulations are carried out under the assumption that both the incident probe and reference optical fields are linearly polarized. In order to quantify the relative differences in polarization and phase, the incidences with respect to the rotating wave frame are configured as $\Omega_{p+}(0) = \Omega_1$, $\Omega_{p-}(0) = \Omega_1$, $\Omega_{r+}(0) = e^{i\theta}\Omega_2$, $\Omega_{r+}(0) = e^{i\theta}e^{i\varphi}\Omega_2$, where real numbers Ω_1, Ω_2 are constant amplitude factors, θ describes the relative phase difference, and φ describes the relative polarization difference.

To study the dynamics in detail, Eq. (7) can be effectively analyzed by Fourier transform, whose details are provided in Appendix C. Nevertheless, the steady-state description of Eq. (8) suffices to provide insight into the features of the system. In the special on-resonance condition of $\Delta = 0$, the emergent probe light intensity can be computed and it contains a succinct term indicative of interference with clear signature from the polarization,

$$\mathrm{Re}\left\{\frac{\Omega_c}{\Omega_d}[\Omega_{r+}(0)\Omega_{p+}^*(0) + \Omega_{r-}(0)\Omega_{p-}^*(0)]\right\}, \tag{10}$$

where the outcome of interference is up to the relative polarization difference of the probe and reference lights and a phase accumulation involving all four optical fields. More generally, Eq. (8) permits two modes of different dynamics with respect to the two eigenvalues of M_0,

$$\lambda_1 = 0, \quad \lambda_2 = \left(-\frac{\Omega_d}{\Omega_c} - \frac{\Omega_c^*}{\Omega_d^*}\right)\Gamma, \tag{11}$$

where λ_1 corresponds to an EIT-like transparency window and λ_2 corresponds to a TLA-like dispersion often with strong dissipation. $\lambda_1 = 0$ implies the existence of nontrivial $\mathbf{e} = [^{e_1}_{e_2}]$ such that $\frac{d}{dz}(e_1^*\Omega_{p\pm} + e_2^*\Omega_{r\pm}) = 0$ which can be recognized as the "dark state." In other words, for the right circularly polarized components of the incidences $\Omega_+(0) = [^{\Omega_{p+}(0)}_{\Omega_{r+}(0)}]$, their projection onto $\mathbf{e}$ is subject to the transparency, which is the same case for the left circularly polarized components of the incidences $\Omega_-(0) = [^{\Omega_{p-}(0)}_{\Omega_{r-}(0)}]$. In particular, we find that both the probe and reference optical fields for the transparency window share the same polarization.

The above observation sketches the inherent characteristics of such a system. Upon the probe and reference incidences of some prescribed initial polarizations and phases, they immediately recombine into two composite optical fields corresponding to two modes of propagation dynamics, respectively. Each mode contains both the probe and reference frequency components. The two modes are typically of dif-

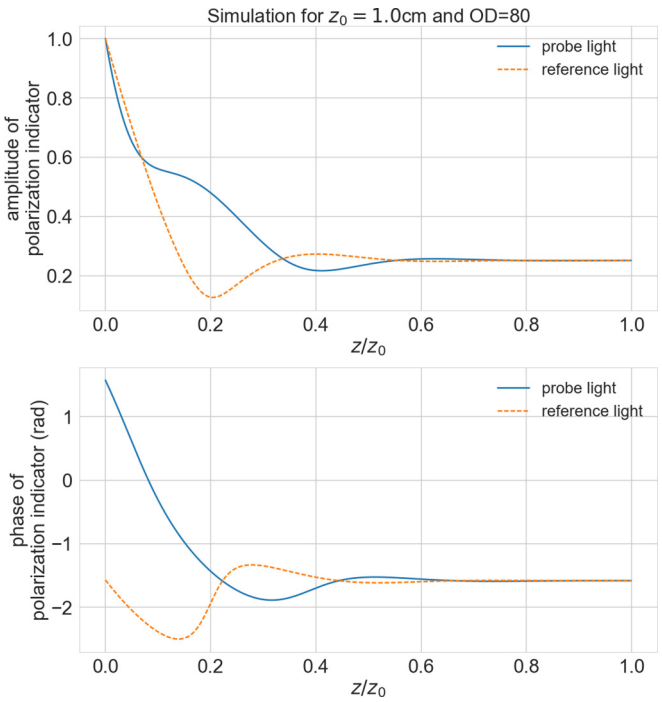

FIG. 7. Numerical simulation for the polarization properties of the dynamics during propagation, where the cold atom ensemble is assumed to be uniformly distributed, of length $z_0 = 1$ cm and OD = 80. The polarization indicator ζ for a general polarization P is defined as $P = \kappa(P_+ + \zeta P_-)$, with $\kappa \equiv (1 + |\zeta|^2)^{-\frac{1}{2}}$, where $P_{+,-}$ are the right and left circular polarization basis. The atomic parameters are $\Gamma = 2\pi \times 6.07$ MHz associated with ^{87}Rb $D2$ transition, $\gamma = 0.01 \times \Gamma$, and the optical parameters are $\Omega_c = \Omega_d = 2\pi \times 5$ MHz, $\Delta = 5$ MHz, together with the incidences $\Omega_{p+}(0) = \Omega_1$, $\Omega_{p-}(0) = i\Omega_1$, $\Omega_{r+}(0) = \Omega_1$, $\Omega_{r-}(0) = -i\Omega_1$, where Ω_1 is a common constant amplitude factor which eventually cancels out. This simulation is carried out under the assumption that the incident probe and reference pulse envelopes are very long; henceforth they can be effectively treated as single frequency optical fields.

ferent dispersion relations and different group velocities: one mode experiences EIT-like transparency, while the other mode experiences TLA-like dispersion. When the incident pulse duration is long enough such that a single frequency description applies, within each mode the polarization states of the probe and reference frequency components are effectively identical. Usually, the TLA-like mode decays away rather rapidly, its energy is dissipated via spontaneous emission, and therefore only one mode of two is emergent from the optically thick cold atom medium. A numerical simulation of the polarization change with the propagation along the z direction is given in Fig. 7.

The derivations so far are essentially within the semiclassical framework, where the probe and reference incidences are assumed to be weak coherent classical optical pulses. Even though the analysis holds for very low incident power, the natural question to ask is whether it makes sense for genuine single-photon incidences. In principle, due to the fact that the EOM Eq. (7) is linear in $\Omega_{p\pm}, \Omega_{r\pm}$ [32], it is anticipated that the polarization-induced interference still exists if both the probe and reference optical fields are quantized. The detailed analysis of this issue is an interesting subject for future work.

IV. CONCLUSION

In conclusion, we have proposed particular forms of atomic linkage structures where the polarization of the optical fields is of essential role in the atom-light interaction. We have shown that the polarization-induced quantum interference comes naturally within the EIT and FWM processes from the double-V and double-M atomic linkage structures. We have also studied the fundamental properties of the polarization-dependent cross-modulation in the double-M structure. We hope that our work helps the effort of realizing strong polarization-dependent nonlinear interactions between weak optical pulses down to the single-photon level in a cold atom medium. We also hope that it helps the research into the polarization degree of freedom from a quantum optics perspective on the topic of stimulated Raman adiabatic passage [35].

ACKNOWLEDGMENTS

The authors acknowledge support by the National Key R&D Program of China (Grant No. 2016YFA0301504). The authors gratefully acknowledge Professor Harold Metcalf who has essentially initiated and cultivated this work. The authors thank Professor Mark Saffman and Dr. Shuyu Zhou for carefully reviewing the manuscript and enlightening discussions.

APPENDIX A: FOUR-STATE SYSTEM WITHOUT DECAYS

Here we choose to analyze the double-V linkage structure which is reconfigured in the format of a topologically equivalent diamond shape shown in Fig. 8 for pedagogical purpose. Moreover, we are going to stick to one major simplification in the discussions of this section: we leave out the spontaneous emission. Then an analytical discussion with a clear picture is allowed, where we put no restriction on the intensities of the two driving lasers: coupling and probe. Before delving into the details, it shall be noted that this interference effect is due to the

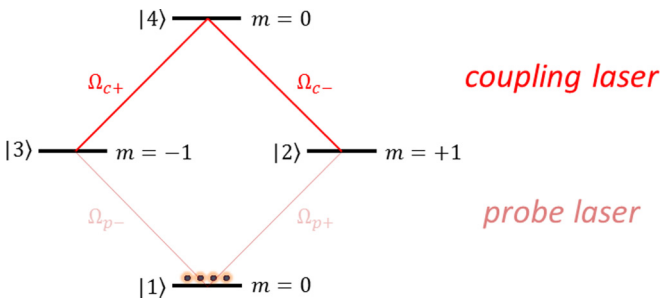

FIG. 8. Level scheme of a diamond shape connection, which is purely artificial and not associated with real atoms. State $|1\rangle$ is in the ground level, states $|2\rangle$ and $|3\rangle$ are in the intermediate level, and state $|4\rangle$ is in the upper level. In reality, the upper level can be recognized as a Rydberg level with long lifetime. The ground level and the intermediate level is coupled by the probe laser, while the intermediate level and the upper level is coupled by the coupling laser.

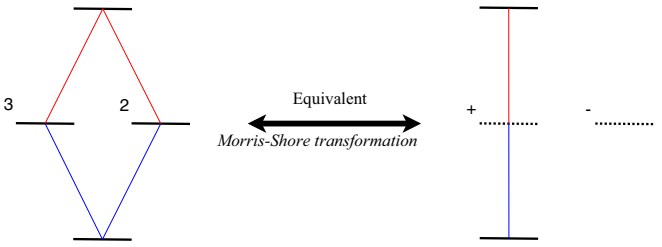

FIG. 9. Reduction of the linkage pattern in the case when the lasers' polarizations are parallel to each other.

quantized angular momentum of the atomic internal electronic states, where the quantum nature of the light does not assume an essential role here. Henceforth a purely semiclassical treatment suffices for the purpose of this section.

We discuss the situation where the probe and coupling lasers driving those transitions have linear polarizations, and we express the polarizations in the circular polarization basis P_+ and P_- as in the following equation, where $|\alpha| = |\beta| = 1$. The relative phase is adjusted with respect to the rotating wave frame associated with Eq. (A2):

$$P_{\text{probe}} = \frac{1}{\sqrt{2}}(P_+ + \alpha P_-), \tag{A1a}$$

$$P_{\text{coupling}} = \frac{1}{\sqrt{2}}(P_+ + \beta P_-). \tag{A1b}$$

And now we can write down the Hamiltonian and solve for the time evolution of the four sublevel total system's wave function, which is $(c_1, c_2, c_3, c_4)^T$ if expressed in the bare states basis. The associated constant phases of the rotating wave frame can always be chosen such that the Rabi frequencies Ω_p and Ω_c are real, where we also include the constant prefactor $\frac{1}{2}$ and $\frac{1}{\sqrt{2}}$. Therefore, we arrive at the following equation:

$$i\frac{d}{dt}\begin{bmatrix} c_1 \\ c_2 \\ c_3 \\ c_4 \end{bmatrix} = \frac{1}{2\sqrt{2}}\begin{bmatrix} 0 & \Omega_p & \alpha\Omega_p & 0 \\ \Omega_p & 0 & 0 & \beta\Omega_c \\ \alpha^*\Omega_p & 0 & 0 & \Omega_c \\ 0 & \beta^*\Omega_c & \Omega_c & 0 \end{bmatrix}\begin{bmatrix} c_1 \\ c_2 \\ c_3 \\ c_4 \end{bmatrix}. \tag{A2}$$

In the situation when the probe and coupling lasers' polarizations are parallel, namely, $\alpha = \beta$, the linkage pattern would reduce to the trivial case as shown in Fig. 9. This reduction is acquired by linearly transforming the states in a process (known as the Morris-Shore transformation) described by Ref. [7], whose method is intended for a two-level system (see also an extension of the original work at Ref. [8]). Explicitly, instead of the two original intermediate sublevels $|2\rangle$ and $|3\rangle$, we describe the system by two newly transformed states $|+\rangle = \frac{1}{\sqrt{2}}(|2\rangle + |3\rangle)$ and $|-\rangle = \frac{1}{\sqrt{2}}(|2\rangle - |3\rangle)$. In this situation, the time evolution described by Eq. (A2) has no difference whether there are two or one substates in the intermediate level. This is also equivalent to a rotation of the coordinate system in Hilbert space.

However, if the probe and coupling lasers' polarizations are orthogonal to each other, namely, $\alpha = 1$ but $\beta = -1$, the situation becomes quite different. A numerical simulation of this situation is shown in Fig. 10, based on Eq. (A2). The population is oscillating back and forth between the ground

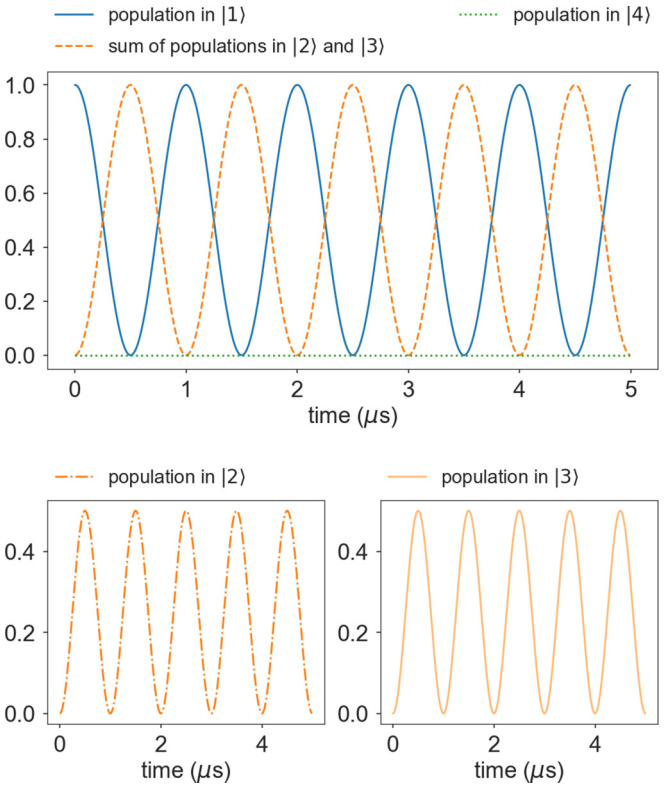

FIG. 10. Numerical simulation of the time evolution of the total four-level system with diamond linkage pattern, when the lasers' polarizations are orthogonal to each other. It is simulating Eq. (A2) with cw lasers, where both Ω_p and Ω_c are set as constants to be $2\pi \times 1$ MHz over the time evolution.

level and the two intermediate sublevels during the time evolution, but never gets transferred to the final level. In other words, the population is trapped and the level $|4\rangle$ becomes dark.

If we apply the same Morris-Shore transformation which leads to Fig. 9, we will have a linkage pattern shown in Fig. 11. We see that the final level $|4\rangle$ together with one of the intermediate states $|-\rangle$ becomes dark if all the population were to start from $|1\rangle$. They stay dark no matter whether the lasers are pulsed or cw. This is solely a consequence of the polarizations' differences between the probe and coupling lasers.

From the linkage reduction mechanisms shown in Fig. 9 and Fig. 11, it is clear that the one-photon detuning won't change the nature of the linkage pattern in these two extreme situations. Namely, when the polarizations are parallel to each

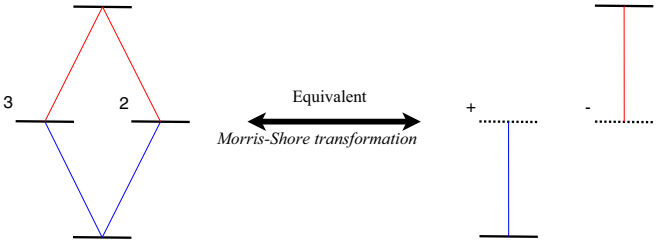

FIG. 11. Reduction of the linkage pattern in the case when the lasers' linear polarizations are orthogonal to each other.

other, the one-photon detuning is acting like it normally does on a three-level system; when the polarizations are orthogonal to each other, the one-photon detuning does nothing because no population can be excited to state $|4\rangle$.

When the two intermediate levels receive probability amplitude pumped by the probe laser from the ground state, they have a phase difference printed onto them by the polarization of the probe laser. If the polarization of the coupling laser is perpendicular to that of the probe laser, then this particular phase of the two intermediate levels makes them dark to the transition corresponding to the coupling laser. The linkage pattern described in Fig. 8 says nothing dictating that $|4\rangle$ shall be trivially dark; the excitation to the final level $|4\rangle$ is made dark by the phase differences induced by the polarizations of the coupling and probe lasers.

For the general case of different linear polarizations, let us first consider the situation where Ω_p and Ω_c are real constants, namely, the lasers are cw. We rewrite Eq. (A2) in a slightly different form to begin with:

$$i\frac{d}{dt}\begin{bmatrix} c_1 \\ c_4 \\ c_2 \\ c_3 \end{bmatrix} = \underbrace{\begin{bmatrix} 0 & 0 & \Omega_p & \alpha\Omega_p \\ 0 & 0 & \beta^*\Omega_c & \Omega_c \\ \Omega_p & \beta\Omega_c & 0 & 0 \\ \alpha^*\Omega_p & \Omega_c & 0 & 0 \end{bmatrix}}_{H_4} \begin{bmatrix} c_1 \\ c_4 \\ c_2 \\ c_3 \end{bmatrix}. \quad \text{(A3)}$$

To examine the time evolution described by Eq. (A3), we look for the eigenstates and eigenvalues of H_4. Then the eigenvalue problem of Eq. (A3) reduces to find a λ to make sure the eigenequation described in Eq. (A4) holds:

$$\lambda\begin{bmatrix} c_1 \\ c_4 \end{bmatrix} = \underbrace{\begin{bmatrix} \Omega_p & \alpha\Omega_p \\ \beta^*\Omega_c & \Omega_c \end{bmatrix}}_{M} \begin{bmatrix} c_2 \\ c_3 \end{bmatrix}, \quad \text{(A4a)}$$

$$\lambda\begin{bmatrix} c_2 \\ c_3 \end{bmatrix} = \underbrace{\begin{bmatrix} \Omega_p & \beta\Omega_c \\ \alpha^*\Omega_p & \Omega_c \end{bmatrix}}_{M^\dagger} \begin{bmatrix} c_1 \\ c_4 \end{bmatrix}. \quad \text{(A4b)}$$

A little observation of the symmetry between (c_1,c_4) and (c_2,c_3) of Eq. (A4) would lead to a simplified eigenvalue problem for 2×2 matrices:

$$\lambda^2\begin{bmatrix} c_1 \\ c_4 \end{bmatrix} = MM^\dagger\begin{bmatrix} c_1 \\ c_4 \end{bmatrix}, \quad \text{(A5a)}$$

$$\lambda^2\begin{bmatrix} c_2 \\ c_3 \end{bmatrix} = M^\dagger M\begin{bmatrix} c_2 \\ c_3 \end{bmatrix}, \quad \text{(A5b)}$$

where $MM^\dagger$ and $M^\dagger M$ are explicitly given in the following formula:

$$MM^\dagger = \begin{bmatrix} 2\Omega_p^2 & (\alpha+\beta)\Omega_p\Omega_c \\ (\alpha^*+\beta^*)\Omega_p\Omega_c & 2\Omega_c^2 \end{bmatrix}, \quad \text{(A6a)}$$

$$M^\dagger M = \begin{bmatrix} \Omega_p^2+\Omega_c^2 & \alpha\Omega_p^2+\beta\Omega_c^2 \\ \alpha^*\Omega_p^2+\beta^*\Omega_c^2 & \Omega_p^2+\Omega_c^2 \end{bmatrix}. \quad \text{(A6b)}$$

Clearly $MM^\dagger$ and $M^\dagger M$ have the same eigenvalues and they are all positive. From the form of $MM^\dagger$ we see that the value of $\alpha+\beta$ determines how much c_1 and c_4 are mixed in the adiabatic states. Let us revisit the two extreme conditions. When α and β are π out of phase, $\alpha+\beta=0$, there is no mixing at all between c_1 and c_4 components, and this case can be viewed as total destructive interference. When α and β are in phase $\alpha=\beta$, the mixing is maximum, and the population transfer rate to the final level $|4\rangle$ is the highest during the time evolution. This can be viewed as constructive interference.

Generally, we can set the criteria for judging how good the excitation is as the time-averaged value of the population in the final state $|4\rangle$, if we assume at the beginning all population is in the ground state $|1\rangle$. Then we ought to look into the time evolution described by Eq. (A3). Like in the case of a simple two-level atom, the time evolution can be found from the adiabatic states of the Hamiltonian in Eq. (A3). Different adiabatic states' time evolutions are different in the sense that they oscillate at different frequencies corresponding to their separate adiabatic energies. As a consequence of taking the time average, those detailed frequencies of the adiabatic states average out. The time-averaged value of the population in the final level $|4\rangle$ is determined by how much population is in the c_4 component of the adiabatic states when the light is turned on when the initial wave function (all population in the ground state $|1\rangle$, bare state) is projected onto the adiabatic states. Roughly speaking, we are to evaluate how much mixing the lasers induce between $|1\rangle$ and $|4\rangle$ in the adiabatic states.

Let us denote the two eigenvalues of $MM^\dagger$ as $\lambda_{MM^\dagger,1}$ and $\lambda_{MM^\dagger,2}$. The mixing depends on the difference $|\lambda_{MM^\dagger,1}-\lambda_{MM^\dagger,2}|$ as in the following equation. The closer $\lambda_{MM^\dagger,1}$ and $\lambda_{MM^\dagger,2}$ comes together, the larger the mixing is:

$$\begin{aligned}&(\lambda_{MM^\dagger,1}-\lambda_{MM^\dagger,2})^2 \\ &\quad = 4\left(\Omega_p^2+\Omega_c^2\right)^2 - 8(1-\mathrm{Re}(\alpha^*\beta))\Omega_p^2\Omega_c^2. \end{aligned} \quad \text{(A7)}$$

Pictorially, the phase differences in the transition amplitudes (in terms of the Rabi frequencies) induced by the different linear polarizations manifest themselves in the excitation process which very much looks like an interference pattern. From this point of view Fig. 8 is just similar to a dual path optical interference experiment, whose paths' phases are determined by the "total sum" of the two lasers' polarizations. Therefore, this effect, nonrigorously speaking, is one example of a Mach-Zehnder interferometer built inside an atom.

The discussion above does not include the effect of spontaneous emission. If the intermediate states $|2\rangle$ and $|3\rangle$ have spontaneous emission channels to decay back to the ground state $|1\rangle$, the basic properties of the above analysis still hold and are serving as the physics backbone of the derived phenomena, just as the discussions in the main text. The reason is that the more chance the atom has at lying at the final excited state $|4\rangle$, the less chance it stays at the lossy intermediate levels and makes a decay. For the general cases including the spontaneous emission, the density-matrix approach is needed. The overall observation is that the physical viewpoint of the interference is appropriate.

APPENDIX B: POLARIZATION-INDUCED INTERFERENCE WITHIN EIT

This section is devoted to the details omitted in the main text for the investigations of systems with the double-V linkage

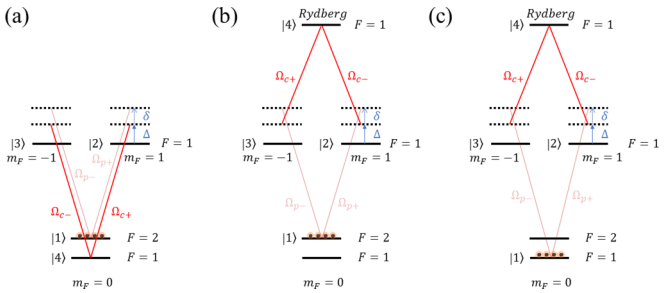

FIG. 12. Different implementation mechanisms for the double-V linkage structure in ^{87}Rb atom, via $D1$ transition. The decay rate of states $|2\rangle$ and $|3\rangle$ is Γ. (a) This is the same type of implementation as Fig. 1(b) of the main text. (b) State $|4\rangle$ is realized by a long-lived Rydberg nS level's $F=1, m_F=0$ state. (c) State $|4\rangle$ is the same as (b), but state $|1\rangle$ is changed to $F=1, m_F=0$. Note that all these three linkage structures share the common symmetry that without the probe and coupling beams they are invariant under the Morris-Shore transform; put in another equivalent way, the atom is not polarized to begin with.

structure. Throughout this section, the discussions are carried out under the rotating wave frame.

Since the phenomena is up to the polarization difference between the probe and coupling beams, or, more specifically, their relative positions on the Poincaré sphere, it is necessary to clarify how the polarization difference between those two optical fields of different frequencies is defined. In other words, since we are describing the polarization state by the circular polarization basis, the issue here is about the relative phase between the basis states. Here we follow the natural choice that the circular basis is derived from the rotating wave frame defined by $|1\rangle,|2\rangle,|3\rangle,|4\rangle$. Namely, once the phase of those atomic states is fixed in the rotating wave frame, the phases of $\Omega_{c+,c-}$ and $\Omega_{p+,p-}$ are unambiguously derived.

In the main text, the implementation of the double-V linkage structure is embedded in the $D1$ transition of ^{87}Rb. In particular, the state $|4\rangle$ is chosen to be one of the clock states of the hyperfine ground level $F=1, m_F=0$. Nevertheless, $|4\rangle$ can also be set as one of the long-lived Rydberg states such that the double-V linkage structure is embedded in a Rydberg EIT system [6] with sublevels, which is illustrated in Fig. 12. In the main text, the polarization of the coupling light is assumed to be linear; yet as long as the coupling light has a fixed polarization state, this assumption is not necessary. In discussions associated with Fig. 12, the coupling light can be in any fixed polarization state.

The EOM corresponding to Fig. 12(a) is

$$\frac{\partial}{\partial z}\Omega_{p+}+\frac{1}{c}\frac{\partial}{\partial t}\Omega_{p+}=i\frac{n\sigma\Gamma}{2}\rho_{21}, \tag{B1a}$$

$$\frac{\partial}{\partial z}\Omega_{p-}+\frac{1}{c}\frac{\partial}{\partial t}\Omega_{p-}=i\frac{n\sigma\Gamma}{2}\rho_{31}, \tag{B1b}$$

$$\frac{d}{dt}\rho_{21}=\frac{i}{2}\Omega_{p+}-\frac{i}{2}\Omega_{c+}\rho_{41}+\left(i(\Delta+\delta)-\frac{\Gamma}{2}\right)\rho_{21}, \tag{B1c}$$

$$\frac{d}{dt}\rho_{31}=\frac{i}{2}\Omega_{p-}+\frac{i}{2}\Omega_{c-}\rho_{41}+\left(i(\Delta+\delta)-\frac{\Gamma}{2}\right)\rho_{31}, \tag{B1d}$$

$$\frac{d}{dt}\rho_{41}=-\frac{i}{2}\Omega_{c+}^{*}\rho_{21}+\frac{i}{2}\Omega_{c-}^{*}\rho_{31}+\left(i\delta-\frac{\gamma}{2}\right)\rho_{41}, \tag{B1e}$$

where γ is the decoherence rate between states $|1\rangle$ and $|4\rangle$.

The EOM corresponding to Fig. 12(b) is

$$\frac{d}{dt}\rho_{21}=\frac{i}{2}\Omega_{p+}+\frac{i}{2}\Omega_{c-}\rho_{41}+\left(i(\Delta+\delta)-\frac{\Gamma}{2}\right)\rho_{21}, \tag{B2a}$$

$$\frac{d}{dt}\rho_{31}=\frac{i}{2}\Omega_{p-}-\frac{i}{2}\Omega_{c+}\rho_{41}+\left(i(\Delta+\delta)-\frac{\Gamma}{2}\right)\rho_{31}, \tag{B2b}$$

$$\frac{d}{dt}\rho_{41}=\frac{i}{2}\Omega_{c-}^{*}\rho_{21}-\frac{i}{2}\Omega_{c+}^{*}\rho_{31}+\left(i\delta-\frac{\gamma}{2}\right)\rho_{41}, \tag{B2c}$$

where we omit the wave equations for $\Omega_{p+,p-}$, which are the same as Eq. (B1), and γ is the decay rate of the Rydberg state $|4\rangle$.

And the EOM corresponding to Fig. 12(c) is

$$\frac{d}{dt}\rho_{21}=\frac{i}{2}\Omega_{p+}+\frac{i}{2}\Omega_{c-}\rho_{41}+\left(i(\Delta+\delta)-\frac{\Gamma}{2}\right)\rho_{21}, \tag{B3a}$$

$$\frac{d}{dt}\rho_{31}=\frac{i}{2}\Omega_{p-}+\frac{i}{2}\Omega_{c+}\rho_{41}+\left(i(\Delta+\delta)-\frac{\Gamma}{2}\right)\rho_{31}, \tag{B3b}$$

$$\frac{d}{dt}\rho_{41}=\frac{i}{2}\Omega_{c-}^{*}\rho_{21}+\frac{i}{2}\Omega_{c+}^{*}\rho_{31}+\left(i\delta-\frac{\gamma}{2}\right)\rho_{41}, \tag{B3c}$$

where we omit the wave equations for $\Omega_{p+,p-}$, which are of the same form of Eq. (B1), but the atom-photon interaction cross section σ is different.

Next, we analyze the dynamics corresponding to Eqs. (B1), (B2), and (B3). Not surprisingly, they share one property in common that two branches of distinct optical propagation and dispersion properties exist, as defined by λ_1,λ_2 in the following equation:

$$\lambda_1=-2\Delta-2\delta-i\Gamma, \tag{B4a}$$

$$\lambda_2=\frac{|\Omega_c|^2}{2\delta+i\gamma}-2\Delta-2\delta-i\Gamma, \tag{B4b}$$

where we define $|\Omega_c|^2=|\Omega_{c+}|^2+|\Omega_{c-}|^2$. λ_1 corresponds to the TLA branch with the dispersion relation $\exp(\frac{i\Gamma}{2\lambda_1}\mathrm{OD})$, while λ_2 corresponds to the EIT branch with the dispersion relation $\exp(\frac{i\Gamma}{2\lambda_2}\mathrm{OD})$, where OD stands for optical depth of the medium.

Define three polarization states in the form of a two-component unit vector with respect to the circular polarization basis as the following:

$$v_1=\frac{1}{|\Omega_c|^2}\begin{bmatrix}-\Omega_{c+}\\ \Omega_{c-}\end{bmatrix},\quad v_2=\frac{1}{|\Omega_c|^2}\begin{bmatrix}-\Omega_{c-}\\ \Omega_{c+}\end{bmatrix},$$
$$v_3=\frac{1}{|\Omega_c|^2}\begin{bmatrix}\Omega_{c-}\\ \Omega_{c+}\end{bmatrix}. \tag{B5}$$

They specify the polarization states corresponding to the EIT branches of the three different configurations Fig. 12(a) and Eq. (B1), Fig. 12(b) and Eq. (B2), and Fig. 12(c) and Eq. (B3),

respectively. Their orthogonal polarization states correspond to the TLA branches accordingly. Loosely speaking, the dark-state polaritons as defined in Ref. [36] are now polarized. The physics of the polarization-induced interference can be explained via the Morris-Shore transform in a rather straightforward manner similar to the discussions in Appendix A. It is also worth mentioning that the relative phase between the probe and coupling lights is involved and implicitly taken care of by the natural choice of the circular polarization basis.

As the next step, we discuss some more details of the analysis for the case where the energy degeneracy between $|2\rangle$ and $|3\rangle$ is lifted, as shown in Fig. 1(c) of the main text. For example, this situation can be generated by a magnetic field along the z direction and therefore the symmetry of the σ^+,σ^- transitions is broken. As stated in the main text, compared with the situation of Fig. 1(a), the unique feature here is that the polarization decomposition into the TLA-like and EIT-like branches varies with the two-photon detuning δ of the probe beam. In order to quantify the effects, we define the polarization indicator ζ for the probe beam with the circular polarization basis as the following equation:

$$P = \kappa(P_+ + \zeta P_-), \quad \text{with } \kappa \equiv (1 + |\zeta|^2)^{-\frac{1}{2}}, \tag{B6}$$

where $\zeta = 0$ corresponds to a purely right circularly polarized light, $\zeta = \infty$ corresponds to a purely left circularly polarized light, and $|\zeta| = 1$ corresponds to linearly polarized light.

The behaviors here can approximately be divided into two categories according to the magnitude of Δ. The first one is when Δ is comparable to or larger than the natural linewidth of the excited state. In this case, the EIT transparency window is relatively narrow and the two branches quickly become strongly left or right circularly polarized when the two-photon detuning $|\delta|$ becomes large. The second one is when Δ is much less than the natural linewidth of the excited state. This case bears more resemblance to the case where $|2\rangle$ and $|3\rangle$ share degenerate energy as stated in Fig. 1(a) of the main text.

A numerical simulation including those two typical cases is presented in Fig. 13. The coupling laser is assumed to be cw at a constant Rabi frequency with a fixed linear polarization $P = P_+ + P_-$. The shift Δ is fixed while the two-photon detuning δ of the probe light is scanned. For each value of δ, two mutually orthogonal polarization states exist, where one corresponds to the EIT-like branch and the other one corresponds to the TLA-like branch. The polarization indicator ζ of the TLA-like branch is included in the figure.

In the main text, a long pulse length condition is imposed upon the incident probe pulse in order to maintain the validity of the steady-state solution. In essence, this condition is not necessary in the discussion of the related phenomena, which means the major observations hold for short probe pulses. The reason is that the probe pulse can always be Fourier transformed into the linear superposition of different frequency components where each single frequency Fourier component is well described by the derivations so far.

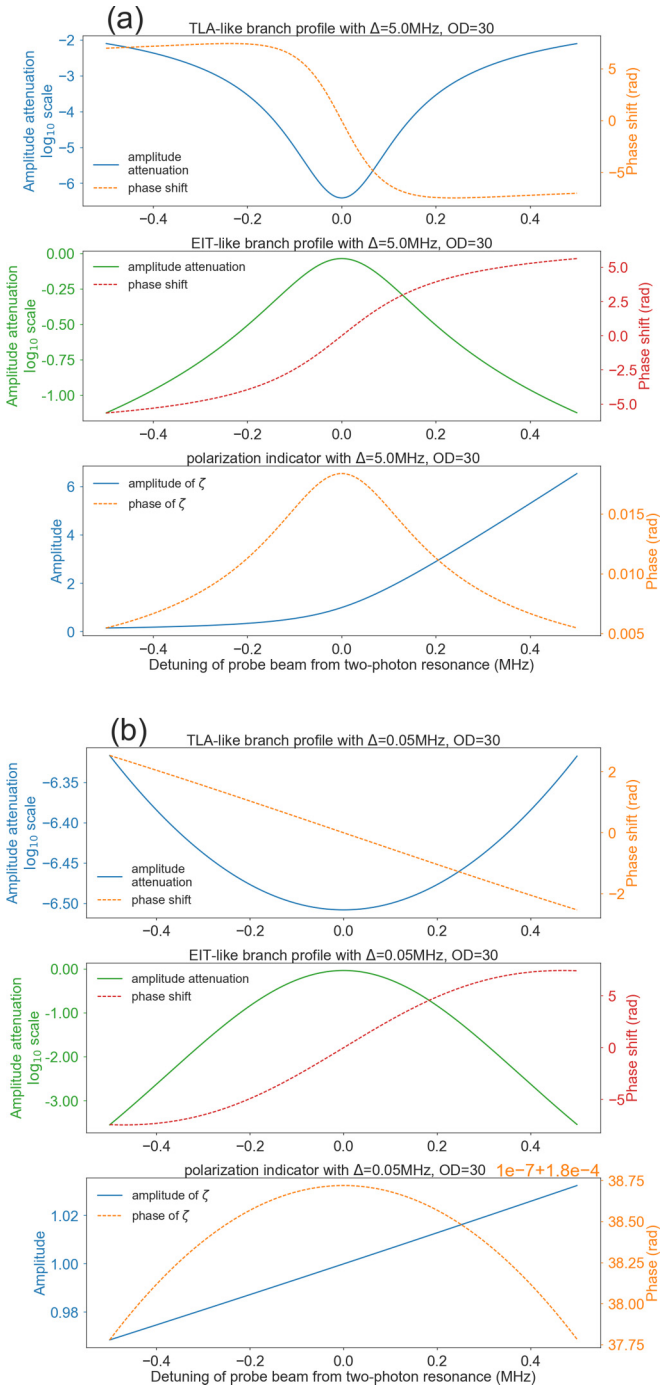

FIG. 13. Numerical simulation for the dispersion of the probe beam after propagation in the optically dense cold atom ensemble (OD = 30), where the atomic structure and coupling laser linkage pattern are according to Fig. 1(c) of the main text. The solid lines are for absorption while the dashed lines are for phase shift. The polarization indicator ζ corresponding to the TLA-like branch is also plotted, which is a complex number. All these simulations are plotted against the probe beam's detuning from the two-photon resonance frequency in MHz, where the focus is put on the neighborhood of the transparency window. The parameters for the simulation are chosen as $\Gamma = 2\pi \times 5.75$ MHz, which is from ^{87}Rb $D1$ transition, $\gamma = 0.001 \times \Gamma$, and $\Omega_c = 2\pi \times 2.5$ MHz. For (a), $\Delta = 2\pi \times 5$ MHz, while for (b) $\Delta = 2\pi \times 0.05$ MHz.

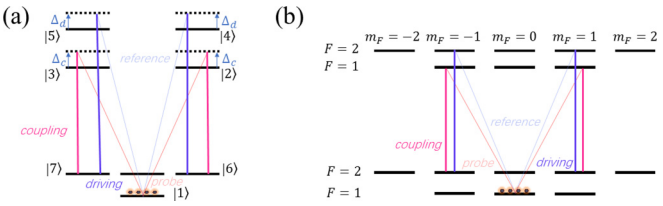

FIG. 14. Implementation of the abstracted double-M linkage structure in ^{87}Rb $D1$ or $D2$ transition, where $|1\rangle$ is set as the the magnetic insensitive clock state $|F = 1, m_F = 0\rangle$.

APPENDIX C: POLARIZATION-INDUCED INTERFERENCE AND CROSS MODULATION IN DOUBLE-M LINKAGE STRUCTURE

In this section we focus on the analysis of the cross modulation via the double-M linkage structure. As stated in the main text, this linkage structure can be realized in a seven-state system based upon ^{87}Rb, as shown in Fig. 14. Even though the discussions thereof are adhering to Fig. 14, it is worth mentioning that a five-state system is also capable of realizing the double-M linkage structure, as shown in Fig. 15.

In the main text, good coherence in the ground-level states have been assumed: $\gamma = 0$; in this section, this assumption is going to be lifted and the decoherence of ρ_{61}, ρ_{71} is to be accounted for. Moreover, the two-photon resonances are assumed to be maintained such that the two-photon detunings are all set to zero. Meanwhile, we also assume that the atoms are cold enough such that the inhomogeneous broadening caused by atomic motion can be neglected. With all these preparations in mind, under a theoretical framework similar to that of Ref. [34], the EOM describing the atom-light system is found as the following equation, as presented in the main text. Naturally, all discussions are carried out under the rotating wave frame where the rotating wave approximation is invoked. The wave fronts of the coupling and driving lasers are assumed to be uniform in phase, and their frequencies are taken as the rotating wave frequencies. Along the z direction, the rotating wave frame basis for the states $|2\rangle, |3\rangle, |4\rangle, |5\rangle, |6\rangle, |7\rangle$ acquire an additional phase term e^{ikz} to account for the probe and reference lights' phase advancing in space, where k is the wave vector:

$$\frac{\partial}{\partial z}\Omega_{p+} + \frac{1}{c}\frac{\partial}{\partial t}\Omega_{p+} = i\frac{n\sigma_p\Gamma_c}{2}\rho_{21}, \tag{C1a}$$

$$\frac{\partial}{\partial z}\Omega_{p-} + \frac{1}{c}\frac{\partial}{\partial t}\Omega_{p-} = i\frac{n\sigma_p\Gamma_c}{2}\rho_{31}, \tag{C1b}$$

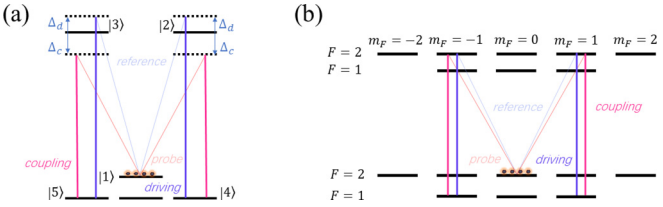

FIG. 15. Implementation of the abstracted double-M linkage structure in ^{87}Rb $D1$ or $D2$ transition with a five-state system, where $|1\rangle$ is set as the magnetic insensitive clock state $|F = 2, m_F = 0\rangle$. Typically this configuration is operated under the condition that $|\Delta_c|, |\Delta_d|$ are large.

$$\frac{\partial}{\partial z}\Omega_{r+} + \frac{1}{c}\frac{\partial}{\partial t}\Omega_{r+} = i\frac{n\sigma_r\Gamma_d}{2}\rho_{41}, \tag{C1c}$$

$$\frac{\partial}{\partial z}\Omega_{r-} + \frac{1}{c}\frac{\partial}{\partial t}\Omega_{r-} = i\frac{n\sigma_r\Gamma_d}{2}\rho_{51}, \tag{C1d}$$

$$\frac{d}{dt}\rho_{21} = \frac{i}{2}\Omega_{p+} + \frac{i}{2}\Omega_c\rho_{61} + \left(i\Delta_c - \frac{\Gamma_c}{2}\right)\rho_{21}, \tag{C1e}$$

$$\frac{d}{dt}\rho_{31} = \frac{i}{2}\Omega_{p-} + \frac{i}{2}\Omega_c\rho_{71} + \left(i\Delta_c - \frac{\Gamma_c}{2}\right)\rho_{31}, \tag{C1f}$$

$$\frac{d}{dt}\rho_{41} = \frac{i}{2}\Omega_{r+} + \frac{i}{2}\Omega_d\rho_{61} + \left(i\Delta_d - \frac{\Gamma_d}{2}\right)\rho_{41}, \tag{C1g}$$

$$\frac{d}{dt}\rho_{51} = \frac{i}{2}\Omega_{r-} + \frac{i}{2}\Omega_d\rho_{71} + \left(i\Delta_d - \frac{\Gamma_d}{2}\right)\rho_{51}, \tag{C1h}$$

$$\frac{d}{dt}\rho_{61} = \frac{i}{2}\Omega_c^*\rho_{21} + \frac{i}{2}\Omega_d^*\rho_{41} - \frac{\gamma}{2}\rho_{61}, \tag{C1i}$$

$$\frac{d}{dt}\rho_{71} = \frac{i}{2}\Omega_c^*\rho_{31} + \frac{i}{2}\Omega_d^*\rho_{51} - \frac{\gamma}{2}\rho_{71}, \tag{C1j}$$

where the meanings of the symbols are the same as stated in the main text.

In order to gain more physical insight into the dynamics in the adiabatic limit, we choose to handle Eq. (C1) via Fourier transform. Suppose that the Fourier transform variable of t is δ, and denote the Fourier-transformed functions as $\widetilde{\cdot}$. Then we arrived at the following equations for $\widetilde{\Omega}_{p+}, \widetilde{\Omega}_{r+}$:

$$\frac{\partial}{\partial z}\widetilde{\Omega}_{p+} - i\frac{\delta}{c}\widetilde{\Omega}_{p+} = i\frac{n\sigma_p\Gamma_c}{2}\widetilde{\rho_{21}}, \tag{C2a}$$

$$\frac{\partial}{\partial z}\widetilde{\Omega}_{r+} - i\frac{\delta}{c}\widetilde{\Omega}_{r+} = i\frac{n\sigma_r\Gamma_d}{2}\widetilde{\rho_{41}}, \tag{C2b}$$

$$0 = \frac{i}{2}\widetilde{\Omega}_{p+} + \frac{i}{2}\Omega_c\widetilde{\rho_{61}} + \left(i\Delta_c + i\delta - \frac{\Gamma_c}{2}\right)\widetilde{\rho_{21}}, \tag{C2c}$$

$$0 = \frac{i}{2}\widetilde{\Omega}_{r+} + \frac{i}{2}\Omega_d\widetilde{\rho_{61}} + \left(i\Delta_d + i\delta - \frac{\Gamma_d}{2}\right)\widetilde{\rho_{41}}, \tag{C2d}$$

$$0 = \frac{i}{2}\Omega_c^*\widetilde{\rho_{21}} + \frac{i}{2}\Omega_d^*\widetilde{\rho_{41}} + \left(i\delta - \frac{\gamma}{2}\right)\widetilde{\rho_{61}}. \tag{C2e}$$

The Fourier transformed equations with $\widetilde{\Omega}_{p-}, \widetilde{\Omega}_{r-}$ are similar to Eq. (C2):

$$\frac{\partial}{\partial z}\widetilde{\Omega}_{p-} - i\frac{\delta}{c}\widetilde{\Omega}_{p-} = i\frac{n\sigma_p\Gamma_c}{2}\widetilde{\rho_{31}}, \tag{C3a}$$

$$\frac{\partial}{\partial z}\widetilde{\Omega}_{r-} - i\frac{\delta}{c}\widetilde{\Omega}_{r-} = i\frac{n\sigma_r\Gamma_d}{2}\widetilde{\rho_{51}}, \tag{C3b}$$

$$0 = \frac{i}{2}\widetilde{\Omega}_{p-} + \frac{i}{2}\Omega_c\widetilde{\rho_{71}} + \left(i\Delta_c + i\delta - \frac{\Gamma_c}{2}\right)\widetilde{\rho_{31}}, \tag{C3c}$$

$$0 = \frac{i}{2}\widetilde{\Omega}_{r-} + \frac{i}{2}\Omega_d\widetilde{\rho_{71}} + \left(i\Delta_d + i\delta - \frac{\Gamma_d}{2}\right)\widetilde{\rho_{51}}, \tag{C3d}$$

$$0 = \frac{i}{2}\Omega_c^*\widetilde{\rho_{31}} + \frac{i}{2}\Omega_d^*\widetilde{\rho_{51}} + \left(i\delta - \frac{\gamma}{2}\right)\widetilde{\rho_{71}}. \tag{C3e}$$

We analyze the symmetry embedded in this system before solving Eqs. (C2) and (C3). Suppose there exists a unitary transform K such that $\widetilde{\Omega}'_p = K\widetilde{\Omega}_p$, $\widetilde{\Omega}'_r =$

$K\widetilde{\Omega}_r$, where $\widetilde{\Omega}_p, \widetilde{\Omega}'_p, \widetilde{\Omega}_r, \widetilde{\Omega}'_r$ are defined in the equation below:

$$\widetilde{\Omega}_p = \widetilde{\Omega}_p(z,\delta) = \begin{bmatrix} \widetilde{\Omega}_{p+} \\ \widetilde{\Omega}_{p-} \end{bmatrix}, \quad \widetilde{\Omega}_r = \widetilde{\Omega}_r(z,\delta) = \begin{bmatrix} \widetilde{\Omega}_{r+} \\ \widetilde{\Omega}_{r-} \end{bmatrix}, \tag{C4a}$$

$$\widetilde{\Omega}'_p = \begin{bmatrix} \widetilde{\Omega}'_{p+} \\ \widetilde{\Omega}'_{p-} \end{bmatrix}, \quad \widetilde{\Omega}'_r = \begin{bmatrix} \widetilde{\Omega}'_{r+} \\ \widetilde{\Omega}'_{r-} \end{bmatrix}. \tag{C4b}$$

The EOM for $\widetilde{\Omega}'_p, \widetilde{\Omega}'_r$ is essentially assuming the identical form of $\widetilde{\Omega}_p, \widetilde{\Omega}_r$, once the following replacements are made:

$$\begin{bmatrix} \widetilde{\rho_{21}} \\ \widetilde{\rho_{31}} \end{bmatrix} \to K \begin{bmatrix} \widetilde{\rho_{21}} \\ \widetilde{\rho_{31}} \end{bmatrix}, \quad \begin{bmatrix} \widetilde{\rho_{41}} \\ \widetilde{\rho_{51}} \end{bmatrix} \to K \begin{bmatrix} \widetilde{\rho_{41}} \\ \widetilde{\rho_{51}} \end{bmatrix}, \quad \begin{bmatrix} \widetilde{\rho_{61}} \\ \widetilde{\rho_{71}} \end{bmatrix} \to K \begin{bmatrix} \widetilde{\rho_{61}} \\ \widetilde{\rho_{71}} \end{bmatrix}. \tag{C5}$$

Essentially, Eqs. (C4) and (C5) summarize a special Morris-Shore transform acting on the $m = +1$ and $m = -1$ states. The fact that the EOM remains invariant under such unitary transforms is a direct consequence of the symmetry in the polarization degree of freedom within the system being considered here. Practically it ensures that there exists no particular polarization orientation for the probe and reference optical fields. All the dynamics associated with the polarization degree of freedom are only up to the relative polarization difference of the incident probe and reference lights.

With the above preparations in mind, we proceed to the formal solutions of Eq. (C2), where the situation with Eq. (C3) is identical. From the last three equations of Eq. (C2), the relation between $\widetilde{\Omega}_{p+}, \widetilde{\Omega}_{r+}$ and $\widetilde{\rho_{21}}, \widetilde{\rho_{41}}$ is readily computed as the following equation:

$$\begin{bmatrix} \widetilde{\Omega}_{p+} \\ \widetilde{\Omega}_{r+} \end{bmatrix} = \underbrace{\begin{bmatrix} \frac{i}{2}\frac{|\Omega_c|^2}{i\delta-\gamma/2} - 2(\Delta_c+\delta) - i\Gamma_c & \frac{i}{2}\frac{\Omega_c\Omega_d^*}{i\delta-\gamma/2} \\ \frac{i}{2}\frac{\Omega_c^*\Omega_d}{i\delta-\gamma/2} & \frac{i}{2}\frac{|\Omega_d|^2}{i\delta-\gamma/2} - 2(\Delta_d+\delta) - i\Gamma_d \end{bmatrix}}_{C(\delta)} \begin{bmatrix} \widetilde{\rho_{21}} \\ \widetilde{\rho_{41}} \end{bmatrix}. \tag{C6}$$

Then substituting $\widetilde{\rho_{21}}, \widetilde{\rho_{41}}$ in Eq. (C2) with Eq. (C6) leads to

$$\frac{\partial}{\partial z}\begin{bmatrix} \widetilde{\Omega}_{p+} \\ \widetilde{\Omega}_{r+} \end{bmatrix} = \underbrace{\left(\frac{i}{2} n\sigma_p \begin{bmatrix} \Gamma_c & 0 \\ 0 & a_r\Gamma_d \end{bmatrix} \begin{bmatrix} \frac{i}{2}\frac{|\Omega_c|^2}{i\delta-\gamma/2} - 2(\Delta_c+\delta) - i\Gamma_c & \frac{i}{2}\frac{\Omega_c\Omega_d^*}{i\delta-\gamma/2} \\ \frac{i}{2}\frac{\Omega_c^*\Omega_d}{i\delta-\gamma/2} & \frac{i}{2}\frac{|\Omega_d|^2}{i\delta-\gamma/2} - 2(\Delta_d+\delta) - i\Gamma_d \end{bmatrix}^{-1} - i\begin{bmatrix} \delta/c & 0 \\ 0 & \delta/c \end{bmatrix} \right)}_{M_0(\delta)} \begin{bmatrix} \widetilde{\Omega}_{p+} \\ \widetilde{\Omega}_{r+} \end{bmatrix}, \tag{C7}$$

which is what we are seeking: the basic equation governing the dynamics on Fourier domain. Also it is worth noting that the quintessence of this system, $M_0(\delta)$, is independent of the properties of incident probe and reference optical fields.

The solution to Eq. (C7) can be formally presented, which applies to the handling of both Eqs. (C2) and (C3):

$$\begin{bmatrix} \widetilde{\Omega}_{p+}(z,\delta) \\ \widetilde{\Omega}_{r+}(z,\delta) \end{bmatrix} = e^{M_0(\delta)z} \begin{bmatrix} \widetilde{\Omega}_{p+}(0,\delta) \\ \widetilde{\Omega}_{r+}(0,\delta) \end{bmatrix},$$
$$\begin{bmatrix} \widetilde{\Omega}_{p-}(z,\delta) \\ \widetilde{\Omega}_{r-}(z,\delta) \end{bmatrix} = e^{M_0(\delta)z} \begin{bmatrix} \widetilde{\Omega}_{p-}(0,\delta) \\ \widetilde{\Omega}_{r-}(0,\delta) \end{bmatrix}, \tag{C8}$$

with the understanding that the incidences to the atomic medium occur at $z = 0$. For the purpose of numerical simulation, evaluation of the inverse Fourier transform at this point yields the result. See Fig. 16 for an example of the case $\delta = 0$, which can also be recognized as the situation where the incident pulse duration is very long such that an effective single-frequency description is adequate.

More specifically, $M_0(\delta)$ can be decomposed via its eigenvalues:

$$M_0(\delta) = T\begin{bmatrix} \chi_1(\delta) & 0 \\ 0 & \chi_2(\delta) \end{bmatrix} T^\dagger, \quad \text{with } T = T(\delta),\ TT^\dagger = I,$$
$$\text{then } e^{M_0(\delta)z} = T\begin{bmatrix} e^{\chi_1(\delta)z} & 0 \\ 0 & e^{\chi_2(\delta)z} \end{bmatrix} T^\dagger, \tag{C9}$$

where $\chi_1(\delta)$ and $\chi_2(\delta)$ correspond to the two modes, respectively. Generally, $\frac{d}{d\delta}\mathrm{Im}(\chi_1)|_{\delta=0} \neq \frac{d}{d\delta}\mathrm{Im}(\chi_2)|_{\delta=0}$; therefore, the group velocities of those two modes are different for narrowband incident pulses.

For a specific Fourier component δ, at any position z, the probe and reference fields can be decomposed into the two modes,

$$\begin{bmatrix} \widetilde{\Omega}_{p+}(z,\delta) \\ \widetilde{\Omega}_{r+}(z,\delta) \end{bmatrix} = l_{+1}e^{\chi_1(\delta)z}\begin{bmatrix} T_{11} \\ T_{21} \end{bmatrix} + l_{+2}e^{\chi_2(\delta)z}\begin{bmatrix} T_{12} \\ T_{22} \end{bmatrix}, \tag{C10}$$

with the projection coefficients l_{+1}, l_{+2} as

$$l_{+1} = T_{11}^*\widetilde{\Omega}_{p+}(0,\delta) + T_{21}^*\widetilde{\Omega}_{r+}(0,\delta),$$
$$l_{+2} = T_{12}^*\widetilde{\Omega}_{p+}(0,\delta) + T_{22}^*\widetilde{\Omega}_{r+}(0,\delta). \tag{C11}$$

The same thing holds for $\widetilde{\Omega}_{p-}(z,\delta), \widetilde{\Omega}_{r-}(z,\delta)$ as well:

$$\begin{bmatrix} \widetilde{\Omega}_{p-}(z,\delta) \\ \widetilde{\Omega}_{r-}(z,\delta) \end{bmatrix} = l_{-1}e^{\chi_1(\delta)z}\begin{bmatrix} T_{11} \\ T_{21} \end{bmatrix} + l_{-2}e^{\chi_2(\delta)z}\begin{bmatrix} T_{12} \\ T_{22} \end{bmatrix}, \tag{C12}$$

with the projection coefficients l_{-1}, l_{-2} as

$$l_{-1} = T_{11}^*\widetilde{\Omega}_{p-}(0,\delta) + T_{21}^*\widetilde{\Omega}_{r-}(0,\delta),$$
$$l_{-2} = T_{12}^*\widetilde{\Omega}_{p-}(0,\delta) + T_{22}^*\widetilde{\Omega}_{r-}(0,\delta). \tag{C13}$$

From Eqs. (C10) and (C12) it is clear that at any Fourier component δ the polarization states for the two modes corresponding to χ_1, χ_2 are well defined, and this is independent of the particular polarization basis by the virtue of the symmetry discussed earlier in Eqs. (C4) and (C4). Meanwhile, we observe that, for each mode of a specific Fourier component δ, the

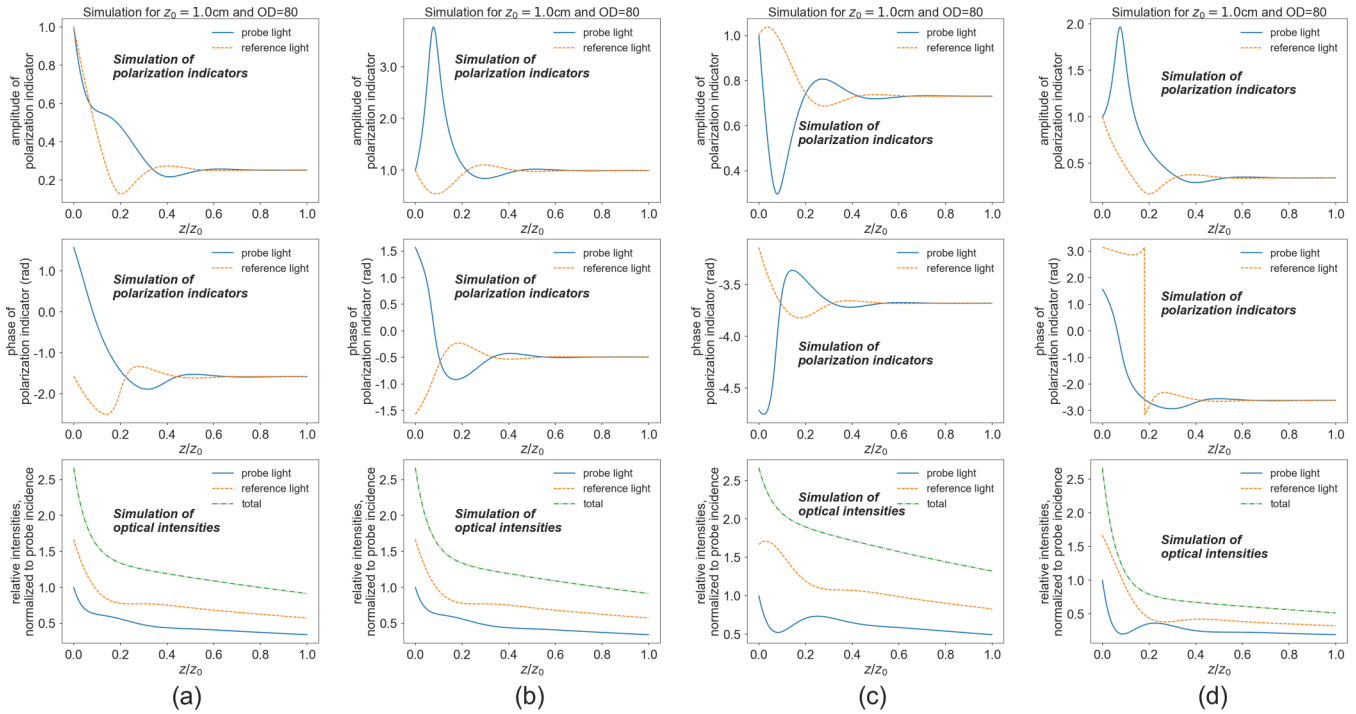

FIG. 16. Numerical simulation for the polarization properties of the dynamics during propagation, where the cold atom ensemble is assumed to be uniformly distributed, of length $z_0 = 1$ cm and OD $= 80$. The polarization indicator ζ is defined in the same way as Eq. (B6), and the intensities of the probe and reference optical fields are also plotted. The simulation is based upon Eqs. (C2) and (C3) for the exact on-resonance Fourier component with $\delta = 0$. All four plots share the same atomic parameters of $\Gamma = 2\pi \times 6.07$ MHz associated with ^{87}Rb $D2$ transition, $\gamma = 0.01 \times \Gamma$, and the optical parameters of $\Omega_c = \Omega_d = 2\pi \times 5$ MHz, $\Delta_c = \Delta_d = 5$ MHz. The incidences are configured differently: (a) $\widetilde{\Omega}_{p+}(0,0) = \Omega_1$, $\widetilde{\Omega}_{p-}(0,0) = i\Omega_1$, $\widetilde{\Omega}_{r+}(0,0) = \Omega_1$, $\widetilde{\Omega}_{r-}(0,0) = -i\Omega_1$; (b) $\widetilde{\Omega}_{p+}(0,0) = \Omega_1$, $\widetilde{\Omega}_{p-}(0,0) = i\Omega_1$, $\widetilde{\Omega}_{r+}(0,0) = i\Omega_1$, $\widetilde{\Omega}_{r-}(0,0) = \Omega_1$; (c) $\widetilde{\Omega}_{p+}(0,0) = \Omega_1$, $\widetilde{\Omega}_{p-}(0,0) = i\Omega_1$, $\widetilde{\Omega}_{r+}(0,0) = \Omega_1$, $\widetilde{\Omega}_{r-}(0,0) = -\Omega_1$; (d) $\widetilde{\Omega}_{p+}(0,0) = \Omega_1$, $\widetilde{\Omega}_{p-}(0,0) = i\Omega_1$, $\widetilde{\Omega}_{r+}(0,0) = i\Omega_1$, $\widetilde{\Omega}_{r-}(0,0) = -i\Omega_1$; where Ω_1 is a common constant amplitude factor.

polarization states of the probe and reference optical fields are the same. Namely, for χ_1, the polarization indicator $\zeta_1 = l_{-1}/l_{+1}$ and, for χ_2, the polarization indicator $\zeta_2 = l_{-2}/l_{+2}$. This observation implies that if the waveform of the probe and reference incidences completely match, which is equivalent to the condition on the Fourier domain that $\frac{\widetilde{\Omega}_{p+}(0,\delta_1)}{\widetilde{\Omega}_{r+}(0,\delta_1)} = \frac{\widetilde{\Omega}_{p+}(0,\delta_2)}{\widetilde{\Omega}_{r+}(0,\delta_2)}$, $\frac{\widetilde{\Omega}_{p-}(0,\delta_1)}{\widetilde{\Omega}_{r-}(0,\delta_1)} = \frac{\widetilde{\Omega}_{p-}(0,\delta_2)}{\widetilde{\Omega}_{r-}(0,\delta_2)}$ for any δ_1,δ_2, then within each mode, the polarization status of the probe and reference optical fields are identical. From this point of view, the asymptotic behavior of Fig. 16 is straightforward to interpret.

In order to gain direct insight into the underlying physics of the system, we now switch gears to derive an analytical solution. For the sake of a simple and succinct expression, we make the assumption that $\Gamma_c = \Gamma_d = \Gamma$, $a_r = 1$, and $|\Omega_c| = |\Omega_d| = \Omega_0$, which means $\Omega_c = e^{i\phi_c}\Omega_0$, $\Omega_d = e^{i\phi_d}\Omega_0$. Then the eigenvalues of the matrix $C(\delta)$ are

$$\lambda_{1,2} = \frac{i}{2}\frac{\Omega_0^2}{i\delta - \gamma/2} - (\Delta_c + \Delta_d) - 2\delta - i\Gamma \pm \sqrt{\left(\frac{i}{2}\frac{\Omega_0^2}{i\delta - \gamma/2}\right)^2 + (\Delta_c - \Delta_d)^2}, \quad \text{(C14)}$$

where we fix the eigenvector for λ_1 as $\mathbf{e} = [{}^{e_1}_{e_2}]$ and the eigenvector for λ_2 as $\mathbf{q} = [{}^{q_1}_{q_2}]$. $\mathbf{e},\mathbf{q}$ are orthogonal to each other $\langle \mathbf{e},\mathbf{q}\rangle = e_1^* q_1 + e_2^* q_2 = 0$ with $|\mathbf{e}| = 1, |\mathbf{q}| = 1$.

Furthermore, when the coupling and driving lasers are strong, the following approximation can be invoked: $\Omega_0 \gg |(i\delta - \gamma/2)(\Delta_c - \Delta_d)|$, which leads to

$$\lambda_1 \approx \frac{\Omega_0^2}{\delta + i\gamma/2} - (\Delta_c + \Delta_d) - 2\delta - i\Gamma,$$
$$\lambda_2 \approx -(\Delta_c + \Delta_d) - 2\delta - i\Gamma, \quad \text{(C15)}$$

where the eigenvectors are also simplified under this approximation:

$$\mathbf{e} \approx \frac{1}{\sqrt{2}}\begin{bmatrix} 1 \\ e^{i(\phi_d - \phi_c)} \end{bmatrix}, \quad \mathbf{q} \approx \frac{1}{\sqrt{2}}\begin{bmatrix} 1 \\ -e^{i(\phi_d - \phi_c)} \end{bmatrix}. \quad \text{(C16)}$$

Therefore, we may name λ_1 as the EIT-like branch and λ_2 as the TLA-like branch with respect to the convention, when there is no confusion. Next, proceeding according to Eq. (C7), while neglecting the relatively much smaller contributions from δ/c,

$$\begin{bmatrix} \widetilde{\Omega}_{p+}(z,\delta) \\ \widetilde{\Omega}_{r+}(z,\delta) \end{bmatrix} = \frac{1}{\sqrt{2}} l_{+1} e^{\frac{i}{2}\frac{n\sigma_p \Gamma z}{\lambda_1}} \begin{bmatrix} 1 \\ e^{i(\phi_d - \phi_c)} \end{bmatrix}$$

$$+\frac{1}{\sqrt{2}}l_{+2}e^{\frac{i}{2}\frac{n\sigma_p\Gamma z}{\lambda_2}}\begin{bmatrix}1\\-e^{i(\phi_d-\phi_c)}\end{bmatrix}, \quad \text{(C17a)}$$

$$\begin{bmatrix}\widetilde{\Omega}_{p-}(z,\delta)\\ \widetilde{\Omega}_{r-}(z,\delta)\end{bmatrix} = \frac{1}{\sqrt{2}}l_{-1}e^{\frac{i}{2}\frac{n\sigma_p\Gamma z}{\lambda_1}}\begin{bmatrix}1\\e^{i(\phi_d-\phi_c)}\end{bmatrix} + \frac{1}{\sqrt{2}}l_{-2}e^{\frac{i}{2}\frac{n\sigma_p\Gamma z}{\lambda_2}}\begin{bmatrix}1\\-e^{i(\phi_d-\phi_c)}\end{bmatrix}, \quad \text{(C17b)}$$

with the projection coefficients $l_{\pm1}$,$l_{\pm2}$ from initial values:

$$l_{\pm1}(\delta) = \frac{1}{\sqrt{2}}[\widetilde{\Omega}_{p\pm}(0,\delta) + e^{-i(\phi_d-\phi_c)}\widetilde{\Omega}_{r\pm}(0,\delta)],$$
$$l_{\pm2}(\delta) = \frac{1}{\sqrt{2}}[\widetilde{\Omega}_{p\pm}(0,\delta) - e^{-i(\phi_d-\phi_c)}\widetilde{\Omega}_{r\pm}(0,\delta)]. \quad \text{(C18)}$$

[1] H. Y. Ling, Y.-Q. Li, and M. Xiao, Phys. Rev. A **53**, 1014 (1996).
[2] Y.-C. Chen, C.-W. Lin, and I. A. Yu, Phys. Rev. A **61**, 053805 (2000).
[3] W. C. Magno, R. B. Prandini, P. Nussenzveig, and S. S. Vianna, Phys. Rev. A **63**, 063406 (2001).
[4] C. Li, Y. Zhang, Z. Nie, Y. Du, R. Wang, J. Song, and M. Xiao, Phys. Rev. A **81**, 033801 (2010).
[5] V. A. Reshetov and I. V. Meleshko, Laser Phys. **24**, 094011 (2014).
[6] S. Bao, H. Zhang, J. Zhou, L. Zhang, J. Zhao, L. Xiao, and S. Jia, Phys. Rev. A **94**, 043822 (2016).
[7] J. R. Morris and B. W. Shore, Phys. Rev. A **27**, 906 (1983).
[8] A. A. Rangelov, N. V. Vitanov, and B. W. Shore, Phys. Rev. A **74**, 053402 (2006).
[9] P.-C. Guan and I. A. Yu, Phys. Rev. A **76**, 033817 (2007).
[10] S. Li, B. Wang, X. Yang, Y. Han, H. Wang, M. Xiao, and K. C. Peng, Phys. Rev. A **74**, 033821 (2006).
[11] F. A. Hashmi and M. A. Bouchene, Phys. Rev. A **77**, 051803 (2008).
[12] T. Lauprêtre, S. Kumar, P. Berger, R. Faoro, R. Ghosh, F. Bretenaker, and F. Goldfarb, Phys. Rev. A **85**, 051805 (2012).
[13] H. Zheng, Y. Zhang, U. Khadka, R. Wang, C. Li, Z. Nie, and M. Xiao, Opt. Express **17**, 15468 (2009).
[14] U. Khadka, Y. Zhang, and M. Xiao, Phys. Rev. A **81**, 023830 (2010).
[15] V. I. Yudin, A. V. Taichenachev, Y. O. Dudin, V. L. Velichansky, A. S. Zibrov, and S. A. Zibrov, Phys. Rev. A **82**, 033807 (2010).
[16] H. Tanji, S. Ghosh, J. Simon, B. Bloom, and V. Vuletić, Phys. Rev. Lett. **103**, 043601 (2009).
[17] Z. Xu, Y. Wu, L. Tian, L. Chen, Z. Zhang, Z. Yan, S. Li, H. Wang, C. Xie, and K. Peng, Phys. Rev. Lett. **111**, 240503 (2013).
[18] M. D. Lukin and A. Imamoğlu, Phys. Rev. Lett. **84**, 1419 (2000).
[19] S. E. Harris and L. V. Hau, Phys. Rev. Lett. **82**, 4611 (1999).
[20] Q. A. Turchette, C. J. Hood, W. Lange, H. Mabuchi, and H. J. Kimble, Phys. Rev. Lett. **75**, 4710 (1995).
[21] H. Tanji-Suzuki, W. Chen, R. Landig, J. Simon, and V. Vuletić, Science **333**, 1266 (2011).
[22] A. Reiserer and G. Rempe, Rev. Mod. Phys. **87**, 1379 (2015).
[23] A. V. Gorshkov, J. Otterbach, M. Fleischhauer, T. Pohl, and M. D. Lukin, Phys. Rev. Lett. **107**, 133602 (2011).
[24] A. C. J. Wade, M. Mattioli, and K. Mølmer, Phys. Rev. A **94**, 053830 (2016).
[25] M. Saffman, T. G. Walker, and K. Mølmer, Rev. Mod. Phys. **82**, 2313 (2010).
[26] S. Li, X. Yang, X. Cao, C. Zhang, C. Xie, and H. Wang, Phys. Rev. Lett. **101**, 073602 (2008).
[27] B.-W. Shiau, M.-C. Wu, C.-C. Lin, and Y.-C. Chen, Phys. Rev. Lett. **106**, 193006 (2011).
[28] Y.-H. Chen, M.-J. Lee, W. Hung, Y.-C. Chen, Y.-F. Chen, and I. A. Yu, Phys. Rev. Lett. **108**, 173603 (2012).
[29] M. Artoni and A. Zavatta, Phys. Rev. Lett. **115**, 113005 (2015).
[30] Z.-Y. Liu, Y.-H. Chen, Y.-C. Chen, H.-Y. Lo, P.-J. Tsai, I. A. Yu, Y.-C. Chen, and Y.-F. Chen, Phys. Rev. Lett. **117**, 203601 (2016).
[31] M. W. Sørensen and A. S. Sørensen, Phys. Rev. A **77**, 013826 (2008).
[32] K. Hammerer, A. S. Sørensen, and E. S. Polzik, Rev. Mod. Phys. **82**, 1041 (2010).
[33] M. Fleischhauer, A. Imamoglu, and J. P. Marangos, Rev. Mod. Phys. **77**, 633 (2005).
[34] L. Deng and M. G. Payne, Phys. Rev. A **71**, 011803 (2005).
[35] Y. Sun and H. Metcalf, Phys. Rev. A **90**, 033408 (2014).
[36] M. Fleischhauer and M. D. Lukin, Phys. Rev. Lett. **84**, 5094 (2000).